HHS Public Access

Author manuscript

Cell Rep. Author manuscript; available in PMC 2019 July 11.

Published in final edited form as:

Cell Rep. 2019 June 18; 27(12): 3422–3432.e4. doi:10.1016/j.celrep.2019.05.058.

Acquired Resistance of EGFR-Mutated Lung Cancer to Tyrosine Kinase Inhibitor Treatment Promotes PARP Inhibitor Sensitivity

Lynnette Marcar[1,6], **Kankana Bardhan**[1,6], **Liliana Gheorghiu**[1], **Patrick Dinkelborg**[1,2], **Heike Pfäffle**[1], **Qi Liu**[1], **Meng Wang**[1], **Zofia Piotrowska**[4], **Lecia V. Sequist**[4], **Kerstin Borgmann**[2], **Jeffrey E. Settleman**[3], **Jeffrey A. Engelman**[3], **Aaron N. Hata**[3,4,5], and **Henning Willers**[1,5,7,*]

[1]Department of Radiation Oncology, Massachusetts General Hospital, Harvard Medical School, Boston, MA 02114, USA

[2]Laboratory of Radiobiology and Experimental Radiooncology, University Hospital Eppendorf, Hamburg 20251, Germany

[3]Center for Cancer Research, Massachusetts General Hospital, Harvard Medical School, Charlestown, MA 02129, USA

[4]Department of Medicine, Massachusetts General Hospital, Harvard Medical School, Boston, MA 02114, USA

[5]Senior author

[6]These authors contributed equally

[7]Lead Contact

SUMMARY

Lung cancers with oncogenic mutations in the epidermal growth factor receptor (EGFR) invariably acquire resistance to tyrosine kinase inhibitor (TKI) treatment. Vulnerabilities of EGFR TKI-resistant cancer cells that could be therapeutically exploited are incompletely understood. Here, we describe a poly (ADP-ribose) polymerase 1 (PARP-1) inhibitor-sensitive phenotype that is conferred by TKI treatment *in vitro* and *in vivo* and appears independent of any particular TKI

*Correspondence: hwillers@partners.org.

AUTHOR CONTRIBUTIONS

Conceptualization, L.M., K. Bardhan, Z.P., L.V.S., J.E.S., J.E.A., A.N.H., and H.W.; Methodology, L.M., K. Bardhan, L.G., M.W., Q.L., and H.W.; Investigation, L.M., K. Bardhan, L.G., P.D., H.P., and M.W.; Resources, L.V.S., J.E.S., J.A.E., and A.N.H.; Writing – Original Draft, L.M., K. Bardhan, and H.W.; Writing – Review & Editing, L.M., L.G., K. Bardhan, P.D., H.P., M.W., Q.L., Z.P., L.V.S., K. Borgmann, J.E.S., J.A.E., A.N.H., and H.W.; Visualization, L.M., L.G., K. Bardhan, and H.W.; Supervision, K. Borgmann, J.A.E., A.N.H., and H.W.

SUPPLEMENTAL INFORMATION

Supplemental Information can be found online at https://doi.org/10.1016/j.celrep.2019.05.058.

DECLARATION OF INTERESTS

K. Bardhan is an employee of Seres Therapeutics. Z.P. receives research support from Novartis, Tesaro, Spectrum, AstraZeneca, and Takeda and has served as a consultant or advisory board member for AstraZeneca, Takeda, Novartis, ImmunoGen, Guardant Health, and Spectrum. L.V.S. is on advisory boards for AstraZeneca, Merrimack, Blueprint Medicines, Genentech, and Janssen, receives research support from AstraZeneca, Novartis, Boehringer-Ingelheim, Genentech, Merrimack, Blueprint Medicines, and LOXO, and receives honoraria from AstraZeneca. J.E.S. is an employee of Calico Life Sciences. J.A.E. is an employee and shareholder of Novartis. A.N.H. receives research support from Novartis, Pfizer, Amgen, and Relay Therapeutics. All other authors declare no competing interests.

resistance mechanism. We find that PARP-1 protects cells against cytotoxic reactive oxygen species (ROS) produced by nicotinamide adenine dinucleotide phosphate (NADPH) oxidase (NOX). Compared to TKI-naive cells, TKI-resistant cells exhibit signs of increased RAC1 activity. PARP-1 catalytic function is required for PARylation of RAC1 at evolutionarily conserved sites in TKI-resistant cells, which restricts NOX-mediated ROS production. Our data identify a role of PARP-1 in controlling ROS levels upon EGFR TKI treatment, with potentially broad implications for therapeutic targeting of the mechanisms that govern the survival of oncogene-driven cancer cells.

Graphical Abstract

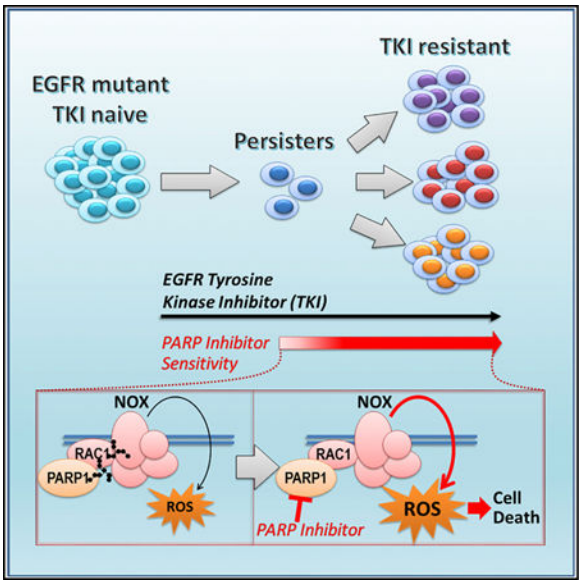

In Brief

Marcar et al. show that epidermal growth factor receptor mutant (EGFRmut) lung cancer cells with acquired resistance to tyrosine kinase inhibitors (TKIs) exhibit PARP-1 dependence for survival. PARP-1 catalytic function is required for PARylation of RAC1, which restricts NOX-mediated production of cytotoxic reactive oxygen species. Findings suggest combining TKI with PARP inhibition in EGFRmut cancers.

INTRODUCTION

In patients with non-small-cell lung cancer (NSCLC) harboring activating mutations in the epidermal growth factor receptor (EGFR), the mainstay of treatment has been administration of an EGFR-directed tyrosine kinase inhibitor (TKI), such as erlotinib, gefinitib, or osimertinib (Mok et al., 2009; Sequist et al., 2008; Soria et al., 2018). However, over time virtually all tumors acquire resistance to TKI through a variety of mechanisms (Jänne et al., 2015; Piotrowska et al., 2015; Sequist et al., 2011). As a result, a majority of patients develop disease progression within 1–2 years. In many cases, mechanisms of acquired resistance remain unknown or cannot be currently targeted (Sequist et al., 2011). Furthermore, more than one resistance mechanism may arise in the same patient (Niederst et

al., 2015). Thus, heterogeneity of acquired TKI resistance is a major clinical problem. Common therapeutic vulnerabilities in EGFR mutant tumors with different TKI resistance (TKI-R) remain to be identified.

Pre-clinical studies have shown that EGFR mutant tumor cells that initially survive TKI treatment can persist and adapt over months to develop bona fide genetic mechanisms of TKI resistance (Hata et al., 2016; Sharma et al., 2010). This ‘‘persister’’ state likely harbors multiple vulnerabilities, which may or may not be relinquished once TKI resistance is acquired (Arasada et al., 2018; Sharma et al., 2010). An unanswered question is whether elimination of these persister cells will substantially delay the development of acquired TKI resistance.

Poly (ADP-ribose) polymerase (PARP) comprises a large family of proteins involved in numerous nuclear and cytoplasmic processes (Bai, 2015; Kraus, 2015). PARP-1 is the most abundant, chromatin-associated enzyme mediating post-translational polyADP-ribosylation (PARylation), which is involved in DNA repair, transcriptional control, genomic stability, cell death, and transformation (Andrabi et al., 2008; Chiu et al., 2011; Peralta-Leal et al., 2009). Since its discovery, most studies have focused on the role of PARP-1 in DNA damage detection and repair (D’Amours et al., 1999). For DNA repair, PARP-1 binds damaged DNA through its N-terminal zinc-finger motifs, thereby activating the C-terminal catalytic domain to hydrolyze NAD+ and produce poly ADP-ribose (PAR) chains (Murai et al., 2012). Over the past decade, however, the role of PARP-1 in gene regulation has received increasing attention (Kraus, 2008; Krishnakumar et al., 2008; Luo and Kraus, 2012). PARP-1 also has been reported to affect mitochondrial content and metabolism as well as reactive oxygen species (ROS) production through controlling the levels of NAD+ and key metabolic transcriptional regulators, including NRF2 (Schiewer and Knudsen, 2014).

Catalytic PARP inhibitors (PARPis) that are in clinical use trap PARP-1/2 on DNA single-strand breaks (SSBs) (Murai et al., 2012). The collision of these complexes with DNA replication forks is synthetically lethal with defects in homologous recombination repair (HRR), such as those conferred by BRCA1/2 mutations (Bryant et al., 2005; Farmer et al., 2005). Additional PARylation targets of PARP-1/2 under conditions of genotoxic stress have been reported, but it is unknown whether they can be therapeutically exploited (Jungmichel et al., 2013). There exists a great need to identify biomarkers of synthetic lethality, other than BRCA1/2 mutations, to guide the rational use of PARPis in cancer patients, including those with lung cancer. In addition, one central question is whether the roles of PARP-1 in processes unrelated to DNA repair impact the anti-cancer activity of PARPis (Lord and Ashworth, 2017).

Because mutation of EGFR can be associated with sensitivity to different DNA damaging agents, including PARPis (Liccardi et al., 2011; Pfäffle et al., 2013), we set out to investigate whether EGFR TKI exposure alters the response of EGFR mutant NSCLC cells to PARPis. We used a panel of established and patient-derived EGFR mutant cell lines that have proven clinically relevant models for studying EGFR TKI resistance mechanisms (Engelman et al., 2007; Hata et al., 2016; Ramirez et al., 2016). Unexpectedly, we find that TKI-R cells are markedly more sensitive to PARPis than their TKI sensitive (TKI-S) controls. We

demonstrate that PARPi hypersensitivity is not linked to HRR but is due to a requirement for PARP-1 to restrict cytotoxic ROS production through PARylation of RAC1 and suppression of nicotinamide adenine dinucleotide phosphate (NADPH) oxidase (NOX) activity. Our data unravel a common vulnerability associated with TKI resistance and the TKI persister state that has potential for clinical translation into future treatments of EGFR mutant lung cancers.

RESULTS

Diverse TKI Resistance Mechanisms Share a Common Sensitivity to PARPis

We subjected a panel of 8 TKI-R EGFR mutant NSCLC cell lines and their TKI-S controls to treatment with the PARPi olaparib (Figure S1A). EGFR TKI resistance was associated with enhanced albeit variable sensitivity to olaparib in 7 of 8 TKI-R cell lines, including patient-derived tumor cell lines, except for H3255GR cells (Figures 1A, 1B, and S1B). Increased PARPi sensitivity was also seen with other clinically relevant inhibitors and confirmed in a colony formation assay (Figures 1C, S2A, and S2B). Furthermore, heterotopic tumor xenografts from established and patient-derived tumor cell lines with acquired TKI resistance demonstrated olaparib sensitivity in contrast to TKI-naive tumors (Figure 1D). In addition, in all TKI-R models except H3255GR cells, there was a significant increase in olaparib-induced γ-H2AX foci compared to TKI-S controls (Figures 1E and 1F). Taken together, PARPi sensitivity that is accompanied by DNA damage is a common phenotype of TKI-R tumors and appears independent of any particular TKI resistance mechanism.

PARPi Sensitivity Can Be Dissociated from PARP Trapping and DNA Repair

Even though PARPis are generally thought to cause cytotoxicity through DNA replication-fork-associated double-strand breaks, we unexpectedly observed large numbers of γ-H2AX foci outside the S- and G2-phase of the cell cycle in cell lines and patient tumor tissue (Figures 2A and 2B). Furthermore, there was no difference in RAD51 foci formation between TKI-R and TKI-S cells (Figure 2C), raising the possibility that PARPi-induced DNA damage was not related to replication forks colliding with PARP molecules trapped on DNA. Indeed, TKI-R cells were sensitive to the PARPi ABT-888, which has relatively little trapping activity (Figure 2D), and when we depleted PARP-1 in TKI-R cells, we observed cytotoxicity that was comparable to olaparib treatment (Figure 2E). Lastly, knock down of PARP-1's partner in base excision and SSB repair, XRCC1, did not abrogate the PARPi sensitivity of TKI-R cells (Figures 2F and S2C). In keeping with this observation, PARPi treatment did not yield any differential increase in DNA breaks in TKI-R compared to TKI-S cells by using the alkaline Comet assay (Figure 2G).

We conclude that the PARPi sensitivity of TKI-R cells is at least partially independent of PARP trapping and SSB repair. To further study the type of DNA damage caused by PARPis, we used a modification of the alkaline Comet assay by using formamidopyrimidine-DNA glycosylase (FPG) to investigate the presence of oxidative damage. We observed a statistically significant increase in FPG-dependent tail moment when TKI-R but not TKI-S cells were treated with olaparib (Figure 2G).

TKI-Resistant Cells Treated with PARPis Display Characteristics of a Pro-oxidant State

Given our data in Figure 2 and because TKI treatment can induce ROS (Okon et al., 2015; Raha et al., 2014), we next investigated ROS levels in our tumor models. There was increased ROS in TKI-R PC9 GR7 cells treated either with PARPis or subjected to PARP-1 depletion (Figures 3A and S3A). A similar phenotype was seen in other TKI-R but not TKI-S cell lines, with the exception of H3255GR cells (Figures 3B and S3B). A similar observation was made in tumor tissues from patients with EGFR mutant cancers, although we do not have matched samples before and after acquisition of TKI resistance in the same patient (Figures 3C and S3C). Notably, even at baseline in the absence of PARPis, ROS were slightly increased in TKI-R compared to TKI-S cells (Figures 3A and S3B). Other signs of a pro-oxidant state in TKI-R cells included susceptibility to olaparib-induced 8-oxoguanine production, presence of EGFR cysteine sulfenylation, protein oxidation, as well as phosphorylation of apoptosis signal-regulating kinase 1 (ASK1) (Figures 3D–3F and S4A). Consistent with the known ROS-mediated activation of ASK1 (Noguchi et al., 2008), olaparib triggered a pronounced apoptotic response in TKI-R but not TKI-S cells (Figures 3G, S4B, and S4C).

Next, we asked whether ROS was the cause of cell death rather than an indirect result of olaparib-induced cytotoxicity. We used the anti-oxidants N-acetyl cysteine and glutathione, which had little to no toxicity under the experimental conditions chosen (Figure S5A). At the selected drug concentrations, these scavengers reduced ROS levels in TKI-R cells and were able to reverse their olaparib sensitivity but did not affect TKI-S cells (Figures 3H and S5B). Although the data do not exclude a contribution of ROS to cell kill at higher doses of olaparib in TKI-S cells, we conclude that PARPi treatment induces cytotoxic ROS in a more pronounced fashion in TKI-R than in TKI-S cells.

PARPi Sensitivity Arises in the TKI Drug Persister State Before TKI Resistance Is Acquired

The observation that TKI-R cell lines demonstrated PARPi sensitivity despite harboring distinct mechanisms of TKI resistance, such as T790M mutation, Met amplification, or epigenetic mechanisms (Figure S1A), suggested that PARPi sensitivity may have arisen before TKI resistance was acquired, i.e., in the early persister state of TKI treatment (Sharma et al., 2010). We, therefore, treated parental TKI-S cells with an EGFR TKI for 0 to 4 weeks and assayed ROS, apoptosis, and cell survival in response to PARPis at different time points. To increase the robustness of our findings, we used different EGFR TKIs (gefitinib and osimertinib) and PARPis (olaparib and niraparib). We observed significant increases in ROS and apoptosis levels upon PARPi exposure by 2 to 3 weeks into TKI treatment (Figures 4A, 4B, S5C, and S5D). At the same time, there was noticeably enhanced cellular sensitivity to PARPis by week 3, as evidence by a sustained shift in drug 50% inhibitory concentration (IC_{50}) values for all treatment combinations (Figures 4C, S6A, and S6B). Further arguing for a TKI-inducible, PARPi sensitive cellular state, we observed that *de novo* TKI-resistant PC9 cells exogenously expressing the T790M resistance mutation can be made PARPi sensitive by mixing the cell population with TKI-S cells and treating with EGFR TKI for 2 weeks (Figure S7A).

To confirm our findings *in vivo*, we used osimertinib and niraparib given that this combination appeared to be the most effective one *in vitro* (Figure 4C; Figure S6B) and because of the increasing importance of osimertinib in the clinic (Soria et al., 2018). PC9 xenografts were induced to regress by treating mice with osimertinib, with the rate of tumor regression starting to plateau after about 3 weeks of treatment (Figure 4D). At that point, animals were randomized to treatment with a PARPi, EGFR TKI, or a combination of the two (Figures 4E and S7B). Strikingly, the addition of TKI to PARPi treatment resulted in a highly statistically significant further tumor regression compared to continued TKI in monotherapy (Figures 4E and S7C). Interestingly, PARPi treatment alone was associated with tumor regrowth within 2 weeks. This observation stands in contrast to our *in vitro* results where the efficacy of PARPi treatment was not influenced by the presence of EGFR TKI, at least not over the 2- to 5-day course of the respective assay (Figures S5C, S5D, S6A, and S6B).

In conclusion, EGFR TKI treatment induces sensitivity to PARPis within ~3 weeks *in vitro* and *in vivo*, which is consistent with the notion that PARPi sensitivity seen in TKI-R resistant models is generally not dictated by the type of acquired TKI resistance mechanism.

PARP-1 Regulates NOX-Dependent ROS through RAC1 PARylation

Turning next toward possible mechanisms of how PARPis may increase ROS, we considered that mitochondria and the NOX family are major sources of cellular ROS (Holmström and Finkel, 2014). Although a mitochondrial ROS scavenger was not able to reduce olaparib-induced ROS (Figure S8A), two different inhibitors of NOX reduced ROS (Figures 5A and S8B). Consistent with this observation, NOX activity in TKI-R cells was enhanced by olaparib treatment (Figure 5B). PARP-1 is a transcriptional regulator of a large number of metabolic regulators, including the redox regulator NRF2 (Wu et al., 2014). However, PARPi did not suppress NRF2 expression in TKI-R cells and produced DNA damage within only 5 h of treatment (Figures S8C and S8D). Therefore, the data suggested a non-transcriptional mechanism of ROS regulation by PARP-1.

To discover protein targets for ROS regulation by PARP-1, we surveyed differentially expressed genes in TKI-R versus TKI-S EGFR mutant cells (Sharma et al., 2010). Interestingly, we observed signs of altered RAC1 pathway activity in TKI-R cells (Figure S9A) potentially linking PARP-1 function to RAC1, a small G-protein in the Rho family, which is an activator of NOX enzymes (Ueyama et al., 2006). Accordingly, the RAC1 protein was expressed at higher levels in TKI-R than in TKI-S cells (Figure S9B). Furthermore, pharmacological inhibition or depletion of RAC1 suppressed PARPi-induced ROS(Figures 5C, S10A, and S10B) and at least partially reversed the PARPi sensitivity of TKI-R cells (Figures 5D, S10C, and S10D).

We then elected to directly investigate whether RAC1 is modulated by PARP-1 catalytic function. In TKI-R cells, RAC1 was PARylated, which could be inhibited by PARPi (Figure 5E). Notably, RAC1 PARylation in TKI-S cells was more pronounced, consistent with lower ROS levels in these cells, but it was resistant to PARPi. We identified several potential PAR-binding consensus motifs in RAC1 that are evolutionary conserved (Figures 5F and S10D). We constructed a panel of loss-of-function RAC1 PARylation mutants, which were

transfected into TKI-R cells, postulating dominant effects over the endogenous protein as described (Farrar et al., 2010). We confirmed that several of these sites, namely amino acids 91, 130–134, and 148, are important for PARP-1-dependent PARylation (Figure 5F). Transfection of the respective PARylation mutants, but not a control mutant (E156A), phenocopied the effects of PARPi with regard to ROS production and cytotoxicity (Figures 5G and 5H). Together, our data demonstrate a role of PARP-1 in regulating NOX complex activity and ROS production in TKI-R cells.

DISCUSSION

PARP-1 is a pleiotropic protein with functions that include regulation of DNA repair, transcription, chromosome organization, mitosis, and metabolism (D'Amours et al., 1999; Luo and Kraus, 2012; Schiewer and Knudsen, 2014). We describe a role of PARP-1 in restricting the production of cytotoxic ROS through controlling PARylation of RAC1 and NOX activity, specifically in EGFR mutant NSCLC cells treated with EGFR TKI. This is not observed in TKI-naive parental cells and appears distinct from PARP-1's canonical function in DNA repair.

ROS are important for cell growth, stress adaption, and cell death in a concentration-dependent manner (Gorrini et al., 2013). Cancer cells often harbor high ROS levels to support proliferation and survival, and yet they may also be more sensitive to any further ROS increase and prone to cell death because of it (Gorrini et al., 2013; Trachootham et al., 2009). Excessive oncogenic ROS production by the NOX complex generates DNA damage with deleterious consequences (Weyemi et al., 2012). Owing to the pleiotropic nature of NOX-derived ROS, tumor cells with upregulated NOX may maintain activated growth pathways, evade cell death, and initiate angiogenesis and metastasis (Block and Gorin, 2012). Accordingly, TKI treatment of EGFR mutant tumor cells is associated with a ROS increase, which may aid in cell survival (Okon et al., 2015; Raha et al., 2014). We speculate that excessive NOX-derived ROS requires these cells to engage protective processes.

RAC1 belongs to the Rho family of small GTPases and plays important roles in G1 cell cycle progression, actin cytoskeleton organization, and downstream gene expression (Heasman and Ridley, 2008; Jaffe and Hall, 2005). RAC1 is spatially and temporally regulated by a wide variety of post-translational modifications, deregulation of which is found in different diseases, including cancer (Hobbs et al., 2015; Levental et al., 2010; Navarro-Lérida et al., 2012; Schwarz et al., 2012). RAC1 PARylation has not been reported previously. We observed that RAC1 is PARylated and that this modification is reduced specifically in TKI-R cells by PARP-1 inhibition within 5 h. Consistent with the reported binding of RAC1 to the NOX complex, which activates NOX enzymes and promotes superoxide production (Ueyama et al., 2006), we found RAC1- and NOX-dependent ROS production in TKI-R but not TKI-S cells. Of note, RAC1-induced superoxide production can induce a feedback loop where RAC1 protein turnover is accelerated by the increased degradation of RAC1 by the ubiquitin-mediated proteasome (Torrino et al., 2011). However, even though PARylation can serve as a signal for the ubiquitination and degradation of PARylated proteins (Huang et al., 2009; Wei and Yu, 2016), we have not observed reduced

RAC1 expression following PARP-1 inhibition in our TKI-R lung cancer cells, suggesting diverse mechanisms of RAC1 regulation.

Our data make an important contribution to the view of PARP-1 as a redox regulator. For example, PARP-1 has been implicated in the regulation of mitochondrial function and oxidative metabolism (Bai et al., 2011). PARP-1 can also promote the transcription of the redox regulator NRF2 (Wu et al., 2014), although in our cell lines we did not find this. In a *Parp-1* knockout mouse model, an increase in ROS levels was seen with age and a significant number of genes linked to oxidative stress and ROS production were dysregulated compared to wild-type mice (Deschênes et al., 2005). Inhibitors of PARP also protect against hydrogen-peroxide-mediated cell death (Cristóvão and Rueff, 1996). However, to date it has been unclear how to exploit these PARP-1 functions for therapeutic gain.

Our data support a concept of synthetic lethality for PARPis that specifically occurs upon TKI treatment in EGFR mutant lung cancer cells. In this model (Figure 5I), PARP-1 functions as a gatekeeper to maintain cell viability by limiting the cellular stress response to TKI exposure by PARylation of RAC1, which serves to restrict NOX-dependent ROS production. As a result, persister cells exhibit PARPi sensitivity within ~3 weeks of TKI treatment, which appears to be preserved even in clones that acquire TKI resistance at a later stage. We thus predict that a fraction of TKI-resistant tumors exhibits some degree of PARPi sensitivity in the clinic. A phase I clinical trial combining a PARPi with an EGFR TKI in TKI-resistant EGFR mutant NSCLC has opened at our institutions (ClinicalTrials.gov: NCT03891615). We suggest that our data have broad implications for a better understanding of metabolic vulnerabilities and acquired TKI resistance not only in EGFR mutant tumors but also potentially in other oncogene-driven cancers.

STAR★METHODS

CONTACT FOR REAGENT AND RESOURCE SHARING

Further information and requests for resources and reagents should be directed to and will be fulfilled by the Lead Contact, Henning Willers (hwillers@partners.org).

EXPERIMENTAL MODEL AND SUBJECT DETAILS

Cell lines—All cell lines have been described previously and are listed in Figure S1A (Crystal et al., 2014; Engelman et al., 2006; Hata et al., 2016; Sharma et al., 2010; Soucheray et al., 2015; Turke et al., 2010). We used 5 TKI-S cell lines, i.e., PC9, HCC827, HCC4006, HCC3255, MGH 119–1, and 8 TKI-R derivatives with different mechanisms of TKI resistance, i.e., PC9 GR7 (drug tolerant/non-T790M), PC9 B (T790M), PC9 C (T790M), HCC827 GR6 (Met amplified), HCC4006 GR6 (EMT driven), HCC3255 GR (T790M), MGH 121–1 (T790M), and MGH 134–1 (T790M). Cell lines were cultured as described (Crystal et al., 2014; Hata et al., 2016; Pfäffle et al., 2013; Sharma et al., 2010; Turke et al., 2010). Established and patient-derived cell lines were cultured in RPMI-1640 (Sigma-Aldrich) except for MGH 119–1 which was cultured in Dulbecco's modified Eagle's medium (DMEM) (Sigma-Aldrich). Cell culture media was supplemented with 10% and

15% Bovine Growth Serum (HyClone) for established and patient-derived cell lines, respectively, 20 mM HEPES (Sigma-Aldrich), 1% penicillin/streptomycin (Sigma-Aldrich), and 2 mM L-Glutamine (Sigma-Aldrich). TKI-R cell lines were maintained in gefitinib (2 mμ) for passaging, but gefitinib was removed when seeding for experiments to facilitate comparisons with TKI-S cells unless specified otherwise. Each cell line was generally kept in passage for no more than 2 months and a passage number window was defined in which the experiments were conducted.

Xenografts—All mouse studies were conducted through Institutional Animal Care and Use Committee–approved animal protocols in accordance with institutional guidelines. Cell line suspensions were prepared in 1:1 matrigel and approximately 5×10^6 cells were injected subcutaneously into the flanks of female athymic nude (Nu/Nu) mice (6–8 weeks old) (Charles River). Visible tumors developed in approximately 2–4 weeks. Tumors were measured with calipers and the tumor volume was calculated according to the formula Vol = 0.52 × L × W2.

Tumor tissues—Tumor tissue explants from NSCLC patients (female) were obtained under Institutional Review Board approved protocol and subjected to *ex vivo* treatment as described (Birkelbach et al., 2013; Willers et al., 2015).

METHOD DETAILS

Drug treatments—Gefitinib, olaparib, ABT-888, osimertinib (LC Laboratories), niraparib (MedKoo Biosciences), rucaparib (Selleck Chemicals), VAS-2870 (Sigma-Aldrich), NSC23766 (Selleck Chemicals), diphenyleneiodonium (DPI) (Sigma-Aldrich) were dissolved in dimethyl sulfoxide following manufacturers' recommendations, and aliquots were stored at −20°C or −80°C. N-Acetyl-L-cysteine (NAC), glutathione, MitoTEMPO, and lucigenin (Sigma-Aldrich) were dissolved in ddH_2O. *In vitro* drug concentrations and incubation times are provided in the Figure legends.

For measuring the effects of olaparib on TKI naive/resistant models *in vivo* (Figure 1), mice with heterotopic xenografts reaching ~350 mm^3 size were randomized to drug versus control groups. Sample size (n = 6–9 per treatment group) was chosen to ensure satisfactory inter-animal reproducibility. For the persister experiment (Figure 4), tumors were grown similarly and mice with established tumors at ~1,000 mm^3 were treated with osimertinib by oral gavage once daily, 5 days a week for 3 weeks until the tumor size reduced to ~350 mm^3 before randomizing them into 3 different drug groups of 7 animals each. Treatments were given by oral gavage once daily, 5 days a week, for an additional 3 weeks. Depending on the experiment, mice which were treated by oral gavage with 50 mg/kg olaparib (LC Laboratories), 50 mg/kg niraparib (MedKoo Biosciences), or/and 5 mg/kg osimertinib (LC Laboratories). Tumor volumes were measured twice weekly for the entire span of the experiment.

NSCLC research specimens not needed for pathological diagnosis were placed into RPMI medium typically within 30 minutes of resection or biopsy and arrived in the laboratory 30–60 minutes later. Specimens were evenly divided into samples of < 5 mm size depending on the amount of tissue available. Samples were mock treated or incubated with olaparib (10

μM) for 24 hours at 37oC and 5% CO_2, followed by flash freezing with OCT (Optimal Cutting Temperature) compound, as described (Birkelbach et al., 2013).

Cell survival assays—Cell proliferation/survival assays were performed as described (Crystal et al., 2014; Hata et al., 2016; Pfäffle et al., 2013). Briefly, exponentially growing cells were seeded into 96-well plates and treated with drug at different concentrations for 5 days, after which fractions of viable cells were determined with the CellTiter-Glo® Luminescent Cell Viability Assay (Promega) following the manufacturer's protocol or with a nucleic acid stain (syto 60, Invitrogen). For clonogenic survival assays, cells were seeded at low density through a limited dilution series and drug was added after ~16 hours. After 2–4 weeks incubation, depending on cell line, viable colonies containing at least 50 cells were counted and the surviving fraction relative to the plating efficiency without drug was determined.

Immunofluorescence microscopy—Cells were fixed with 4% paraformaldehyde for 15 minutes and then permeabilized with PBS/0.5% Triton-X for 20 minutes at 4°C. Cells were blocked for one hour at room temperature with 5% goat serum/PBS. Primary antibodies γ-H2AX (Millipore) and RAD51 (Santa Cruz) were added for 2 hours at room temperature in 3% goat serum/PBS/0.1%Triton-X and subsequently incubated with fluorescent secondary antibody Alexa488 (Invitrogen) or Alexa555 (Invitrogen) for 1 hour at room temperature. For costaining experiments, cells were incubated with anti-53BP1 rabbit polyclonal antibody and anti-PCNA mouse monoclonal antibody (Abcam). Nuclei were counterstained with DAPI and subnuclear protein foci were scored by fluorescence microscopy (Olympus BX51). Primary antibody rabbit polyclonal anti-53BP1 (Abcam) and mouse monoclonal anti-PCNA (Abcam) were added for 24 hours at 4°C and secondary antibody Alexa Fluor488 goat anti-mouse (Invitrogen) and Alexa Fluor555 goat anti-rabbit (Invitrogen) were added for 1 hr at room temperature. Nuclei were stained with DAPI (1 μg/ml in ddH2O) for 2 minutes and subnuclear foci were scored by fluorescence microscopy (Olympus BX51). For measurement of oxidative DNA damage, fixed cells were stained with anti 8-oxoguanine mouse monoclonal antibody (Millipore). For cell-based ROS measurements, cryosections were incubated with CellROX reagent (Molecular Probes/Thermo Scientific) at a final concentration of 5 μM in PBS, incubated for 30 minutes at 37°C, followed by fixing in 3.7% formaldehyde for 15 minutes. Samples were air-dried and mounted with ProLong Diamond Antifade Mountant (Molecular Probes/Thermo Scientific) with DAPI, allowed to cure for 21 hours and imaged within 3 hours. For ROS measurements, random images were analyzed by NIS-Elements AR (Nikon). Nuclear regions of interest (ROI) were defined and average fluorescence staining intensity per ROI recorded while normalizing for unspecific extracellular staining.

Antibodies and western blot—SDS-PAGE and western blotting was carried out using standard procedures. Primary antibodies against EGFR (Santa Cruz), PARP-1 (Cell Signaling), XRCC1 (Cell Signaling), PAR (Trevigen), RAC1 (Millipore), NRF2 (Santa Cruz), Actin (Santa Cruz), Tubulin, Lamin A (Millipore) were used. Horseradish peroxidase (HRP)-conjugated rabbit anti-mouse and goat anti-rabbit secondary antibodies were purchased from Santa Cruz.

Immunoprecipitation (IP)—Cells were lysed in IP buffer (50mM Tris-HCl [pH 7.5], 150mM NaCl, 1% (v/v) NP-40, and protease inhibitor (Roche)) for 30 minutes on ice, centrifuged for 10 minutes at 13,000 x g and supernatant was removed for analysis. The lysate was then pre-cleared with 40 μL slurry of protein G beads (Santa Cruz) for 45 minutes at 4°C, centrifuged for 3 minutes at 2,000 x g and the beads were discarded and the supernatant removed for IP. A total of 500–1,000 mg of protein was incubated with 1–2 μg/ml of antibody overnight at 4°C and immunoprecipitated the following day with 40 mL slurry of protein G beads (Santa Cruz) for 2 hours at 4° C. Precipitates were washed three times for 5 minutes in IP buffer at 4°C before addition of SDS-gel-loading buffer and immunoprecipitated proteins were detected by western blot. In case of IP Rac and Probe Rac, the secondary antibody used was Mouse TrueBlot® ULTRA: Anti-Mouse Ig HRP (Rockland antibodies & assays) without hindrance by interfering immunoprecipitating immunoglobulin heavy and light chains.

RNA interference—siRNA knockdown was performed using X-tremeGENE siRNA transfection reagent (Roche) and validated siRNA sequences (working concentration 200 nM) against PARP-1 (Santa Cruz), RAC1 (Millipore Sigma), and XRCC1 (Ambion) for 48 hours. A scramble sequence (Ambion) was used as a negative control.

Fpg-modified alkaline Comet assay—Oxidative DNA damage was detected using *E. coli* Formamidopyrimidine-DNA Glycosylase (Fpg) in conjunction with the CometAssay® single cell gel electrophoresis kit (Trevigen). Tail moment was analyzed using TriTek CometScore.

Detection of DNA and protein oxidation—Oxidative DNA damage was detected by treating cells with 10 μM olaparib for 24 hours, or hydrogen peroxide as a control, followed by fixation with 25% Acetic Acid/75%MeOH for 20 minutes at −20° C and permeabilization with 0.5% Triton-X buffer for 10 minutes at room temperature. Cells were stained with mouse monoclonal anti-8-oxoguanine antibody (Millipore) in 3% goat serum (1:200). As a secondary antibody goat anti-mouse Alexa Fluor 488 (1:1,000) was used. Oxidized proteins were detected using the OxyBlot Protein Oxidation Detection Kit (Millipore) according to the manufacturer's instructions.

S-Sulfenylation assay—Cells were lysed in lysis buffer (50 mM HEPES, 50 mM NaCl, 1 mM EDTA, 10% glycerol,1% Triton x-100) supplemented with 0.5 mM DCP-BIO1, 0.1 mM N-ethyl malemide, 0.1 mM Iodacetamide, 1 mM Na_3VO_4 and protease inhibitors. Samples were sonicated, kept on ice for 30 minutes, and centrifuged at 12,000 x g for 10 minutes at 4°C. The pellet was discarded and the supernatant removed to a new tube and rotated for 1 hour at room temperature to allow for labeling of sulfenic acids. After incubation, protein was precipitated by acetone to remove any excess probe and pelleted by centrifuging at 12,000 x g for 5 minutes. The pellet was washed in 70% acetone and suspended in lysis buffer. The amount of protein was determined by the BCA assay and 1 mg of total protein was added to a 50 μL slurry of streptavidin beads. Then, beads were rotated overnight at 4°C. After 24 hours, beads were centrifuged at 1,000 x g for 3 minutes, supernatant was discarded, and beads were washed in 1 μL of lysis buffer. This washing step

was repeated three times and beads were eluted in 30 mL of 2 x LDS buffer (Life Technologies) supplemented with 2-ME.

Flow cytometry—To measure ROS in cells, 2′, 7′ dichlorodihydrofluorescein diacetate (H2DCF-DA) fluorescent probe (Invitrogen) was employed at a concentration of 10 μM and detected by flow cytometry (SORP 4 Laser BD LSRII (BD Biosciences)) using standard protocol (Ameziane-El-Hassani and Dupuy, 2013). For quantification of apoptosis, cells and media were collected, centrifuged, and resuspended in Annexin binding buffer with cell density adjusted to approximately 10^6/mL 48 hours after treatment with olaparib. Cells were stained with propidium iodide (Sigma-Aldrich) and Annexin V–Cy5 following the manufacturer's protocol (BioVision), and then analyzed by flow cytometry.

NADPH assay—NOX Activity was measured using lucigenin as a substrate. Lucigenin is a reagent that interacts with superoxide and generates luminescence. This emitted luminescence can be quantitatively recorded and analyzed by a luminometer. Cell were treated with (5 μM) and without Olaparib for 5 hours and harvested in ice cold phosphate buffer of 50 mM KH2PO4, 1 mM EGTA, and 150 mM sucrose (pH 7.4) with protease inhibitors. Cell homogenates (~50 ml) were incubated with 100 μM NADPH (Sigma-Aldrich) in the absence or presence of ROS inhibitor DPI (1 μM) for 20 minutes at 37°C. Lucigenin (50 μM) was added to the reaction mixture and the incubation continued for 20 minutes. Luminescence was read by the MultiLabel reader, 2140 Envision (Perkin Elmer) as relative-light units (RLU) and activity was normalized to protein concentration.

Generation of RAC1 mutants—RAC-1 mutagenesis was performed by site-directed mutagenesis using the Stratagene Quick-Change system according to the manufacturer's instructions. All DNAs were sequenced to verify that only the desired mutations were present.

QUANTIFICATION AND STATISTICAL ANALYSIS

Information on experimental replicates can be found in each Figure legend. Statistical comparisons were performed with the Student's t test (two-sided) unless otherwise stated.

Supplementary Material

Refer to Web version on PubMed Central for supplementary material.

ACKNOWLEDGMENTS

This study was funded by the Dana-Farber/Harvard Cancer Center SPORE in Lung Cancer grant P50CA090578 (J.E.S. and H.W.), an American Lung Association Lung Cancer Discovery Award LCD400286 (H.W.), K08CA197389 (A.N.H.), and R01CA137008 (L.V.S.). The authors are grateful to John M. Hourihan and Chake Takadjian for technical assistance.

REFERENCES

Ameziane-El-Hassani R, and Dupuy C (2013). Detection of Intracellular Reactive Oxygen Species (CM-H2DCFDA). Bio-protocol 3, e313.

Andrabi SA, Dawson TM, and Dawson VL (2008). Mitochondrial and nuclear cross talk in cell death: parthanatos. Ann. N Y Acad. Sci 1147, 233–241. [PubMed: 19076445]

Arasada RR, Shilo K, Yamada T, Zhang J, Yano S, Ghanem R, Wang W, Takeuchi S, Fukuda K, Katakami N, et al. (2018). Notch3-dependent β-catenin signaling mediates EGFR TKI drug persistence in EGFR mutant NSCLC. Nat. Commun 9, 3198. [PubMed: 30097569]

Bai P (2015). Biology of Poly(ADP-Ribose) Polymerases: The Factotums of Cell Maintenance. Mol. Cell 58, 947–958. [PubMed: 26091343]

Bai P, Cantó C, Oudart H, Brunyánszki A, Cen Y, Thomas C, Yamamoto H, Huber A, Kiss B, Houtkooper RH, et al. (2011). PARP-1 inhibition increases mitochondrial metabolism through SIRT1 activation. Cell Metab 13, 461–468. [PubMed: 21459330]

Birkelbach M, Ferraiolo N, Gheorghiu L, Pfäffle HN, Daly B, Ebright MI, Spencer C, O'Hara C, Whetstine JR, Benes CH, et al. (2013). Detection of impaired homologous recombination repair in NSCLC cells and tissues. J. Thorac. Oncol 8, 279–286. [PubMed: 23399959]

Block K, and Gorin Y (2012). Aiding and abetting roles of NOX oxidases in cellular transformation. Nat. Rev. Cancer 12, 627–637. [PubMed: 22918415]

Bryant HE, Schultz N, Thomas HD, Parker KM, Flower D, Lopez E, Kyle S, Meuth M, Curtin NJ, and Helleday T (2005). Specific killing of BRCA2-deficient tumours with inhibitors of poly(ADP-ribose) polymerase. Nature 434, 913–917. [PubMed: 15829966]

Chiu LY, Ho FM, Shiah SG, Chang Y, and Lin WW (2011). Oxidative stress initiates DNA damager MNNG-induced poly(ADP-ribose)polymerase-1-dependent parthanatos cell death. Biochem. Pharmacol 81, 459–470. [PubMed: 21056551]

Cristóvão L, and Rueff J (1996). Effect of a poly(ADP-ribose) polymerase inhibitor on DNA breakage and cytotoxicity induced by hydrogen peroxide and gamma-radiation. Teratog. Carcinog. Mutagen 16, 219–227. [PubMed: 9381409]

Crystal AS, Shaw AT, Sequist LV, Friboulet L, Niederst MJ, Lockerman EL, Frias RL, Gainor JF, Amzallag A, Greninger P, et al. (2014). Patient-derived models of acquired resistance can identify effective drug combinations for cancer. Science 346, 1480–1486. [PubMed: 25394791]

D'Amours D, Desnoyers S, D'Silva I, and Poirier GG (1999). Poly(ADP-ribosyl)ation reactions in the regulation of nuclear functions. Biochem. J 342, 249–268. [PubMed: 10455009]

Deschênes F, Massip L, Garand C, and Lebel M (2005). In vivo misregulation of genes involved in apoptosis, development and oxidative stress in mice lacking both functional Werner syndrome protein and poly(ADP-ribose) polymerase-1. Hum. Mol. Genet 14, 3293–3308. [PubMed: 16195394]

Engelman JA, Mukohara T, Zejnullahu K, Lifshits E, Borrás AM, Gale CM, Naumov GN, Yeap BY, Jarrell E, Sun J, et al. (2006). Allelic dilution obscures detection of a biologically significant resistance mutation in EGFR-amplified lung cancer. J. Clin. Invest 116, 2695–2706. [PubMed: 16906227]

Engelman JA, Zejnullahu K, Mitsudomi T, Song Y, Hyland C, Park JO, Lindeman N, Gale CM, Zhao X, Christensen J, et al. (2007). MET amplification leads to gefitinib resistance in lung cancer by activating ERBB3 signaling. Science 316, 1039–1043. [PubMed: 17463250]

Farmer H, McCabe N, Lord CJ, Tutt AN, Johnson DA, Richardson TB, Santarosa M, Dillon KJ, Hickson I, Knights C, et al. (2005). Targeting the DNA repair defect in BRCA mutant cells as a therapeutic strategy. Nature 434, 917–921. [PubMed: 15829967]

Farrar D, Rai S, Chernukhin I, Jagodic M, Ito Y, Yammine S, Ohlsson R, Murrell A, and Klenova E (2010). Mutational analysis of the poly(ADP-ribosyl)ation sites of the transcription factor CTCF provides an insight into the mechanism of its regulation by poly(ADP-ribosyl)ation. Mol. Cell. Biol 30, 1199–1216. [PubMed: 20038529]

Gorrini C, Harris IS, and Mak TW (2013). Modulation of oxidative stress as an anticancer strategy. Nat. Rev. Drug Discov 12, 931–947. [PubMed: 24287781]

Hata AN, Niederst MJ, Archibald HL, Gomez-Caraballo M, Siddiqui FM, Mulvey HE, Maruvka YE, Ji F, Bhang HE, Krishnamurthy Radhakrishna V, et al. (2016). Tumor cells can follow distinct evolutionary paths to become resistant to epidermal growth factor receptor inhibition. Nat. Med 22, 262–269. [PubMed: 26828195]

Heasman SJ, and Ridley AJ (2008). Mammalian Rho GTPases: new insights into their functions from in vivo studies. Nat. Rev. Mol. Cell Biol 9, 690–701. [PubMed: 18719708]

Hobbs GA, Mitchell LE, Arrington ME, Gunawardena HP, DeCristo MJ, Loeser RF, Chen X, Cox AD, and Campbell SL (2015). Redox regulation of Rac1 by thiol oxidation. Free Radic. Biol. Med 79, 237–250. [PubMed: 25289457]

Holmström KM, and Finkel T (2014). Cellular mechanisms and physiological consequences of redox-dependent signalling. Nat. Rev. Mol. Cell Biol 15, 411–421. [PubMed: 24854789]

Huang SM, Mishina YM, Liu S, Cheung A, Stegmeier F, Michaud GA, Charlat O, Wiellette E, Zhang Y, Wiessner S, et al. (2009). Tankyrase inhibition stabilizes axin and antagonizes Wnt signalling. Nature 461, 614–620. [PubMed: 19759537]

Jaffe AB, and Hall A (2005). Rho GTPases: biochemistry and biology. Annu. Rev. Cell Dev. Biol 21, 247–269. [PubMed: 16212495]

Jänne PA, Yang JC, Kim DW, Planchard D, Ohe Y, Ramalingam SS, Ahn MJ, Kim SW, Su WC, Horn L, et al. (2015). AZD9291 in EGFR inhibitor-resistant non-small-cell lung cancer. N. Engl. J. Med 372, 1689–1699. [PubMed: 25923549]

Jungmichel S, Rosenthal F, Altmeyer M, Lukas J, Hottiger MO, and Nielsen ML (2013). Proteome-wide identification of poly(ADP-Ribosyl)ation targets in different genotoxic stress responses. Mol. Cell 52, 272–285. [PubMed: 24055347]

Kraus WL (2008). Transcriptional control by PARP-1: chromatin modulation, enhancer-binding, coregulation, and insulation. Curr. Opin. Cell Biol 20, 294–302. [PubMed: 18450439]

Kraus WL (2015). PARPs and ADP-Ribosylation: 50 Years … and Counting. Mol. Cell 58, 902–910. [PubMed: 26091339]

Krishnakumar R, Gamble MJ, Frizzell KM, Berrocal JG, Kininis M, and Kraus WL (2008). Reciprocal binding of PARP-1 and histone H1 at promoters specifies transcriptional outcomes. Science 319, 819–821. [PubMed: 18258916]

Levental I, Lingwood D, Grzybek M, Coskun U, and Simons K (2010). Palmitoylation regulates raft affinity for the majority of integral raft proteins. Proc. Natl. Acad. Sci. USA 107, 22050–22054. [PubMed: 21131568]

Liccardi G, Hartley JA, and Hochhauser D (2011). EGFR nuclear translocation modulates DNA repair following cisplatin and ionizing radiation treatment. Cancer Res 71, 1103–1114. [PubMed: 21266349]

Lord CJ, and Ashworth A (2017). PARP inhibitors: Synthetic lethality in the clinic. Science 355, 1152–1158. [PubMed: 28302823]

Luo X, and Kraus WL (2012). On PAR with PARP: cellular stress signaling through poly(ADP-ribose) and PARP-1. Genes Dev 26, 417–432. [PubMed: 22391446]

Mok TS, Wu YL, Thongprasert S, Yang CH, Chu DT, Saijo N, Sunpaweravong P, Han B, Margono B, Ichinose Y, et al. (2009). Gefitinib or carboplatin-paclitaxel in pulmonary adenocarcinoma. N. Engl. J. Med 361, 947–957. [PubMed: 19692680]

Murai J, Huang SY, Das BB, Renaud A, Zhang Y, Doroshow JH, Ji J, Takeda S, and Pommier Y (2012). Trapping of PARP1 and PARP2 by Clinical PARP Inhibitors. Cancer Res 72, 5588–5599. [PubMed: 23118055]

Navarro-Lérida I, Sánchez-Perales S, Calvo M, Rentero C, Zheng Y, Enrich C, and Del Pozo MA (2012). A palmitoylation switch mechanism regulates Rac1 function and membrane organization. EMBO J 31, 534–551. [PubMed: 22157745]

Niederst MJ, Sequist LV, Poirier JT, Mermel CH, Lockerman EL, Garcia AR, Katayama R, Costa C, Ross KN, Moran T, et al. (2015). RB loss in resistant EGFR mutant lung adenocarcinomas that transform to small-cell lung cancer. Nat. Commun 6, 6377. [PubMed: 25758528]

Noguchi T, Ishii K, Fukutomi H, Naguro I, Matsuzawa A, Takeda K, and Ichijo H (2008). Requirement of reactive oxygen species-dependent activation of ASK1-p38 MAPK pathway for extracellular ATP-induced apoptosis in macrophage. J. Biol. Chem 283, 7657–7665. [PubMed: 18211888]

Okon IS, Coughlan KA, Zhang M, Wang Q, and Zou MH (2015). Gefitinib-mediated reactive oxygen specie (ROS) instigates mitochondrial dysfunction and drug resistance in lung cancer cells. J. Biol. Chem 290, 9101–9110. [PubMed: 25681445]

Peralta-Leal A, Rodríguez-Vargas JM, Aguilar-Quesada R, Rodríguez MI, Linares JL, de Almodóvar MR, and Oliver FJ (2009). PARP inhibitors: new partners in the therapy of cancer and inflammatory diseases. Free Radic. Biol. Med 47, 13–26. [PubMed: 19362586]

Pfäffle HN, Wang M, Gheorghiu L, Ferraiolo N, Greninger P, Borgmann K, Settleman J, Benes CH, Sequist LV, Zou L, and Willers H (2013). EGFR-activating mutations correlate with a Fanconi anemia-like cellular phenotype that includes PARP inhibitor sensitivity. Cancer Res 73, 6254–6263. [PubMed: 23966292]

Piotrowska Z, Niederst MJ, Karlovich CA, Wakelee HA, Neal JW, Mino-Kenudson M, Fulton L, Hata AN, Lockerman EL, Kalsy A, et al. (2015). Heterogeneity Underlies the Emergence of EGFRT790 Wild-Type Clones Following Treatment of T790M-Positive Cancers with a Third-Generation EGFR Inhibitor. Cancer Discov 5, 713–722. [PubMed: 25934077]

Raha D, Wilson TR, Peng J, Peterson D, Yue P, Evangelista M, Wilson C, Merchant M, and Settleman J (2014). The cancer stem cell marker aldehyde dehydrogenase is required to maintain a drug-tolerant tumor cell sub-population. Cancer Res 74, 3579–3590. [PubMed: 24812274]

Ramirez M, Rajaram S, Steininger RJ, Osipchuk D, Roth MA, Morinishi LS, Evans L, Ji W, Hsu CH, Thurley K, et al. (2016). Diverse drug-resistance mechanisms can emerge from drug-tolerant cancer persister cells. Nat. Commun 7, 10690. [PubMed: 26891683]

Schiewer MJ, and Knudsen KE (2014). Transcriptional roles of PARP1 in cancer. Mol. Cancer Res 12, 1069–1080. [PubMed: 24916104]

Schwarz J, Proff J, Hävemeier A, Ladwein M, Rottner K, Barlag B, Pich A, Tatge H, Just I, and Gerhard R (2012). Serine-71 phosphorylation of Rac1 modulates downstream signaling. PLoS One 7, e44358. [PubMed: 22970203]

Sequist LV, Martins RG, Spigel D, Grunberg SM, Spira A, Jänne PA, Joshi VA, McCollum D, Evans TL, Muzikansky A, et al. (2008). First-line gefitinib in patients with advanced non-small-cell lung cancer harboring somatic EGFR mutations. J. Clin. Oncol 26, 2442–2449. [PubMed: 18458038]

Sequist LV, Waltman BA, Dias-Santagata D, Digumarthy S, Turke AB, Fidias P, Bergethon K, Shaw AT, Gettinger S, Cosper AK, et al. (2011). Genotypic and histological evolution of lung cancers acquiring resistance to EGFR inhibitors. Sci. Transl. Med 3, 75ra26.

Sharma SV, Lee DY, Li B, Quinlan MP, Takahashi F, Maheswaran S, McDermott U, Azizian N, Zou L, Fischbach MA, et al. (2010). A chromatin-mediated reversible drug-tolerant state in cancer cell subpopulations. Cell 141, 69–80. [PubMed: 20371346]

Soria JC, Ohe Y, Vansteenkiste J, Reungwetwattana T, Chewaskulyong B, Lee KH, Dechaphunkul A, Imamura F, Nogami N, Kurata T, et al.; FLAURA Investigators (2018). Osimertinib in Untreated EGFR-Mutated Advanced Non-Small-Cell Lung Cancer. N. Engl. J. Med 378, 113–125. [PubMed: 29151359]

Soucheray M, Capelletti M, Pulido I, Kuang Y, Paweletz CP, Becker JH, Kikuchi E, Xu C, Patel TB, Al-Shahrour F, et al. (2015). Intratumoral Heterogeneity in EGFR-Mutant NSCLC Results in Divergent Resistance Mechanisms in Response to EGFR Tyrosine Kinase Inhibition. Cancer Res 75, 4372–4383. [PubMed: 26282169]

Torrino S, Visvikis O, Doye A, Boyer L, Stefani C, Munro P, Bertoglio J, Gacon G, Mettouchi A, and Lemichez E (2011). The E3 ubiquitin-ligase HACE1 catalyzes the ubiquitylation of active Rac1. Dev. Cell 21, 959–965. [PubMed: 22036506]

Trachootham D, Alexandre J, and Huang P (2009). Targeting cancer cells by ROS-mediated mechanisms: a radical therapeutic approach? Nat. Rev. Drug Discov 8, 579–591. [PubMed: 19478820]

Turke AB, Zejnullahu K, Wu YL, Song Y, Dias-Santagata D, Lifshits E, Toschi L, Rogers A, Mok T, Sequist L, et al. (2010). Preexistence and clonal selection of MET amplification in EGFR mutant NSCLC. Cancer Cell 17, 77–88. [PubMed: 20129249]

Ueyama T, Geiszt M, and Leto TL (2006). Involvement of Rac1 in activation of multicomponent Nox1- and Nox3-based NADPH oxidases. Mol. Cell. Biol 26, 2160–2174. [PubMed: 16507994]

Wei H, and Yu X (2016). Functions of PARylation in DNA Damage Repair Pathways. Genomics Proteomics Bioinformatics 14, 131–139. [PubMed: 27240471]

Weyemi U, Lagente-Chevallier O, Boufraqech M, Prenois F, Courtin F, Caillou B, Talbot M, Dardalhon M, Al Ghuzlan A, Bidart JM, et al. (2012). ROS-generating NADPH oxidase NOX4 is

a critical mediator in oncogenic H-Ras-induced DNA damage and subsequent senescence. Oncogene 31, 1117–1129. [PubMed: 21841825]

Willers H, Gheorghiu L, Liu Q, Efstathiou JA, Wirth LJ, Krause M, and von Neubeck C (2015). DNA Damage Response Assessments in Human Tumor Samples Provide Functional Biomarkers of Radiosensitivity. Semin. Radiat. Oncol 25, 237–250. [PubMed: 26384272]

Wu T, Wang XJ, Tian W, Jaramillo MC, Lau A, and Zhang DD (2014). Poly(ADP-ribose) polymerase-1 modulates Nrf2-dependent transcription. Free Radic. Biol. Med 67, 69–80. [PubMed: 24140708]

Highlights

- TKI resistance promotes PARP inhibitor sensitivity of EGFR mutant lung cancer cells
- PARP inhibitor sensitivity can be traced back to the initial TKI persister state
- PARP inhibitor sensitivity is mediated by NOX-dependent reactive oxygen species
- Abrogating PARylation of NOX activator RAC1 phenocopies PARP inhibitor effects

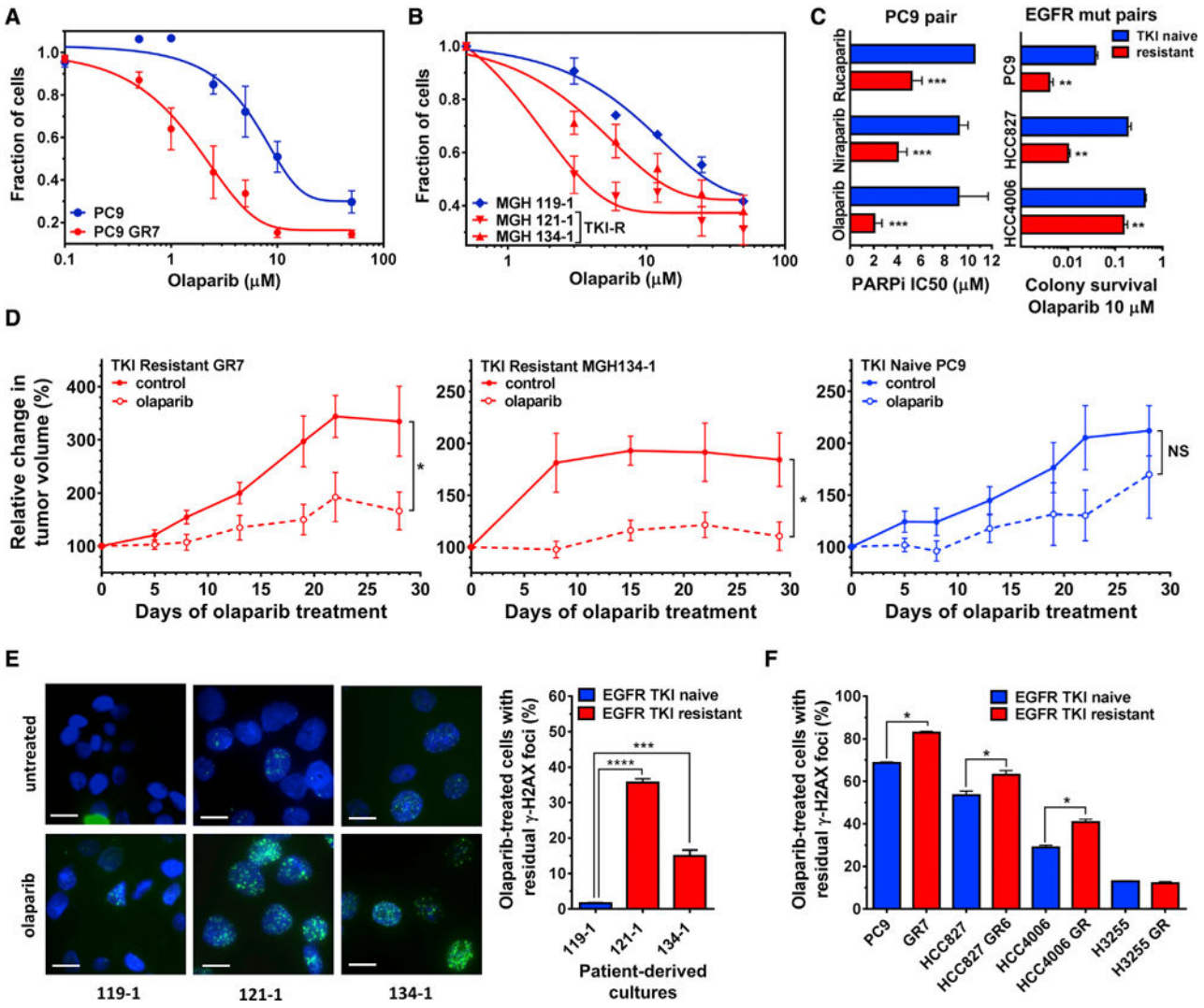

Figure 1. PARP Inhibitor Sensitivity of EGFR Mutant TKI-Resistant (TKI-R) Cells *In Vitro* and *In Vivo*

(A and B) Fraction of PC9 cells (A) and patient-derived cell lines (B) after 5 days of treatment with olaparib at the concentrations shown. Gefitinib-resistant lines are marked as GR or TKI-R.

(C) Left, IC_{50} values for different PARPis in the PC9/GR7 pair. Right, clonogenic survival of different TKI-S/R pairs following PARPi treatment.

(D) Growth of heterotopic TKI-R and TKI-S EGFR mutant NSCLC xenografts as a result of PARPi or vehicle treatment.

(E) Left, representative immunofluorescence microscopy images showing DNA damage in patient-derived cell lines caused by olaparib (2.5 μM). Green, γ-H2AX; blue, 4′,6-diamidino-2-phenylindole (DAPI). Scale bars, 20 μm. Right, percentage of cells with ≥20 γ-H2AX foci after 24 h of olaparib.

(F) Percentage of cells with ≥20 γ-H2AX foci after 24 h of olaparib. Data points and error bars represent means with SE based on ≥3 biological repeats with at least 2 to 3 technical repeats in the cell survival experiments and 6 to 9 tumors per data point in the mouse

experiments. In the immunofluorescence experiments, each repeat is based on 50 to 100 nuclei per data point.

*p ≤ 0.05, **p ≤ 0.01, ***p ≤ 0.001, ****p ≤ 0.0001.

See also Figures S1 and S2.

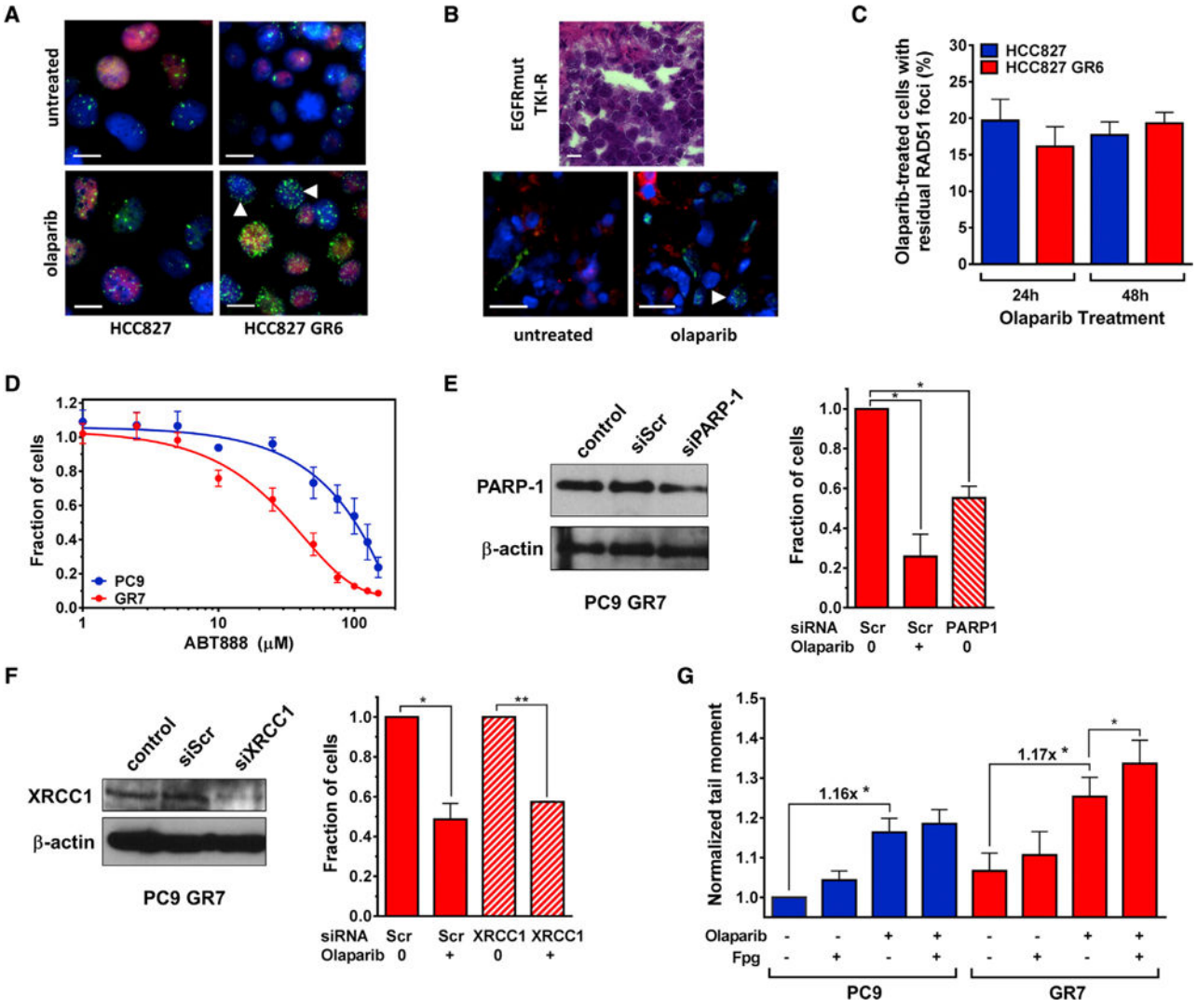

Figure 2. Dissociation of PARPi Effects from PARP Trapping and DNA Repair

(A) Representative images of DNA damage (green, 53BP1) in cells in different phases of the cell cycle (red, PCNA positive = S- and G2-phase). White arrows indicate PCNA-negative cells that are in G1 phase. Scale bars, 20 μm.

(B) Representative images of tumor explant tissue taken from a patient with EGFR mutant TKI-R disease. Top, 40× image with hematoxylin and eosin staining showing viable tumors cells. Bottom, 53BP1 and PCNA co-staining as in (A). Scale bars, 20 μm.

(C) Percentage of cells with at least 10 RAD51 foci following treatment with olaparib (2.5 μM) for 24 or 48 h.

(D) Fraction of cells after 5-day treatment with the PARPi ABT-888.

(E) Left, western blot depicting partial depletion of PARP-1 by using validated small interfering RNA (siRNA) in PC9 GR7 cells. Right, fraction of cells after treatment with 5 μM olaparib or after partial depletion of PARP-1.

(F) Left, western blot depicting knock down of XRCC1 with validated siRNA in PC9 GR7 cells. Right, fraction of cells after treatment with 5 μM olaparib with or without XRCC1 depletion.

(G) Normalized tail moment in a modified alkaline Comet assay, with or without FPG treatment, following 24-h treatment of cells with olaparib (5 μM). Data points and error bars represent means with SE based on ≥3 biological repeats with ≥3 technical repeats. In the immunofluorescence experiments, each repeat is based on 50 to 100 nuclei per data point. *$p \leq 0.05$, **$p \leq 0.01$.
See also Figure S2.

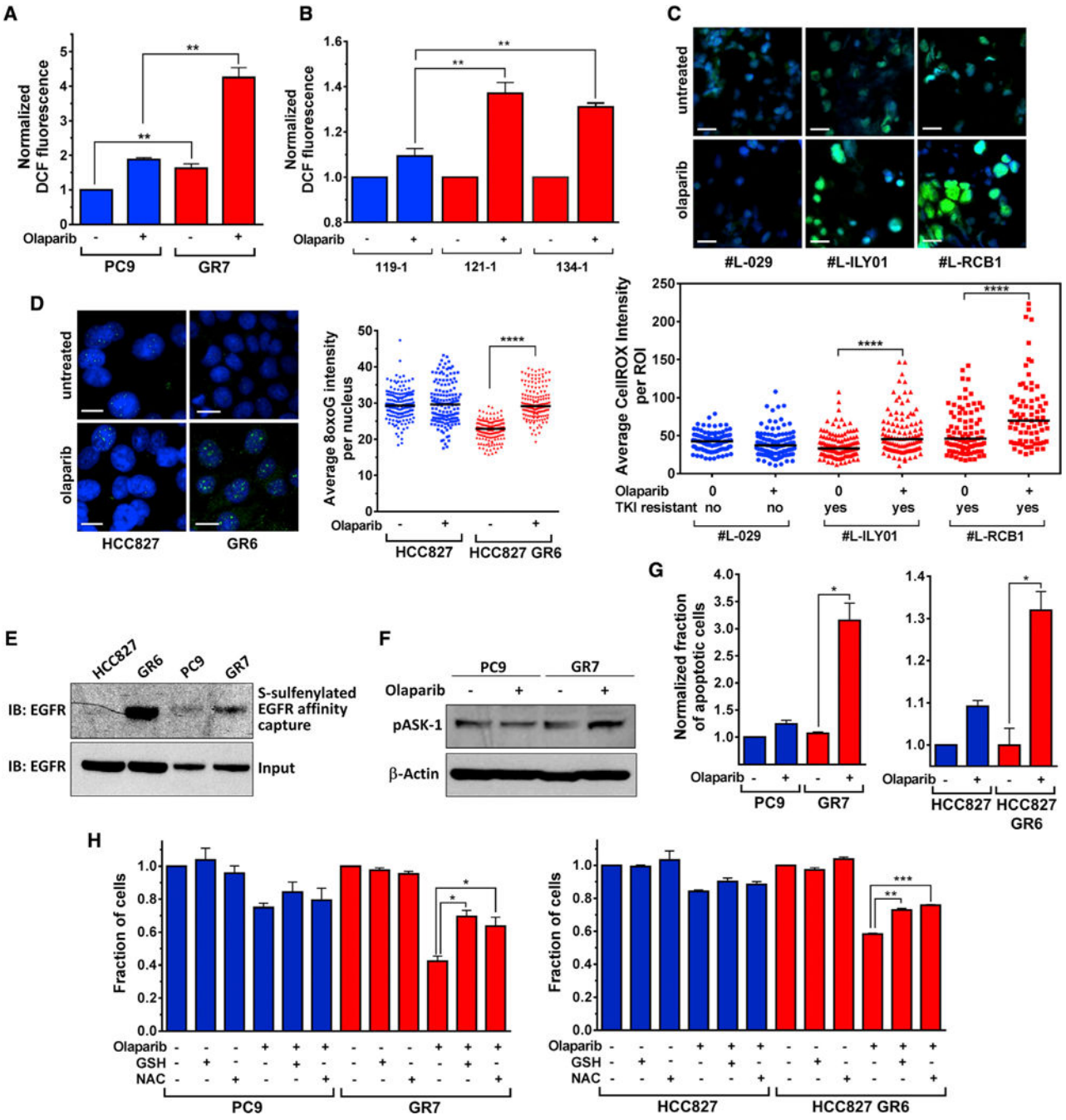

Figure 3. PARP Inhibition Increases ROS and Oxidative Damage in TKI-R Cells

(A and B) Normalized 2',7'-dichlorofluorescein (DCF) fluorescence as a measure of intracellular ROS after treatment of PC9 cells (A) and patient-derived cell lines (B) with olaparib (10 μM for 24 h) followed by incubation with 2′,7′-dichloro-dihydrofluorescein diacetate for 30 min and flow cytometry.

(C) Top panel, representative immunofluorescence microscopy images showing CellRox staining of patient tumor tissue explants after 24 h of olaparib treatment (10 μM). Scale bars, 20 μm. Bottom, average CellRox intensity per nuclear region of interest (ROI) in tumor

explants as a function of olaparib treatment and acquired EGFR TKI resistance. Horizontal lines present median, and statistical comparison by Mann-Whitney test.

(D) Left, representative images showing olaparib-induced oxidative DNA damage (8-oxoguanine) in TKI-R versus TKI-S cells. Right, average 8-oxoguanine (8oxoG) staining intensity per nucleus in HCC827 cells. Scale bars, 20 μm.

(E) Sulfenylation assay on TKI-S and TKI-R cell lines as shown.

(F) Western blot showing phosphorylation of ASK after 24-h treatment with olaparib (5 μM).

(G) Fraction of apoptotic cells normalized to untreated TKI-S controls as measured by annexin V after 48 h of olaparib (10 μM).

(H) Fraction of TKI-S and TKI-R cells following treatments with olaparib (5 μM), glutathione (1 μM), or N-acetyl-L-cysteine (NAC; 400 nM) for 5 days as indicated. Data points and error bars represent means with SE based on ≥3 biological repeats with ≥3 technical repeats in the cell survival experiments. For the flow-cytometry-based experiments, each sample was run once. For the immunofluorescence experiments, the total number of nuclei counted is displayed.

*$p \leq 0.05$, **$p \leq 0.01$, ***$p \leq 0.001$, ****$p \leq 0.0001$.

See also Figures S3, S4, and S5.

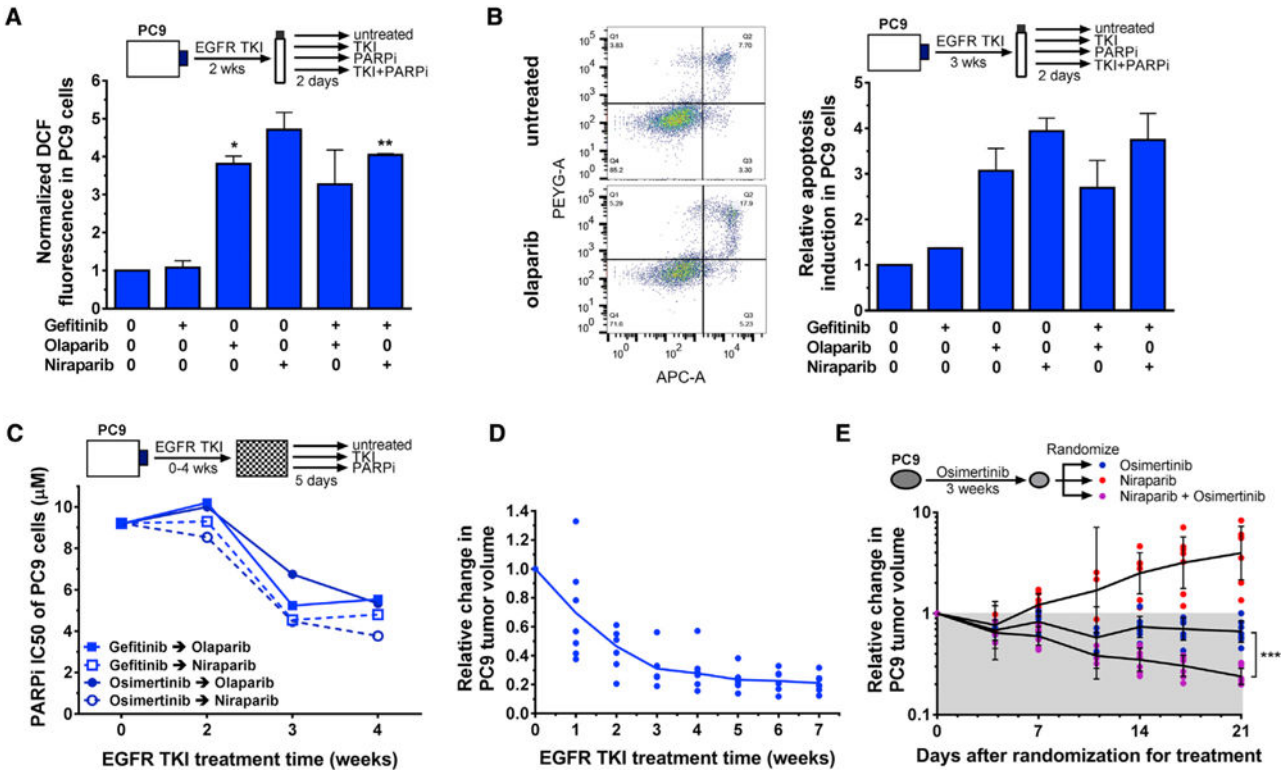

Figure 4. PARPi Sensitivity Induced During the Initial Response to EGFR TKI

(A) DCF fluorescence measured in TKI-S PC9 cells after 2 weeks of 1-μM gefitinib treatment followed by reseeding and 48 h of 5-μM PARPi treatment with or without continued gefitinib.

(B) Left, representative flow cytometry diagrams of propidium iodide and annexin V double-stained cells after 3 weeks of 1-μM gefitinib treatment followed by reseeding and 48 h of 5-μM PARPi treatment with or without continued gefitinib. Right, relative fold induction of apoptosis compared to untreated controls.

(C) IC_{50} values for 5-day treatment with 2 different PARPis plotted against preceding treatment with different EGFR TKIs for up to 4 weeks in TKI-S PC9 cells.

(D) Relative tumor growth of heterotopic PC9 xenografts treated with osimertinib.

(E) Relative tumor growth of PC9 xenografts pre-treated with osimertinib for 3 weeks following randomization to one of three treatment groups as shown. Data points and error bars represent means with SE based on ≥3 biological repeats with ≥3 technical repeats and 7 tumors per data point in the mouse experiments.

*p ≤ 0.05, **p ≤ 0.01, ***p ≤ 0.001.

See also Figures S5, S6, and S7.

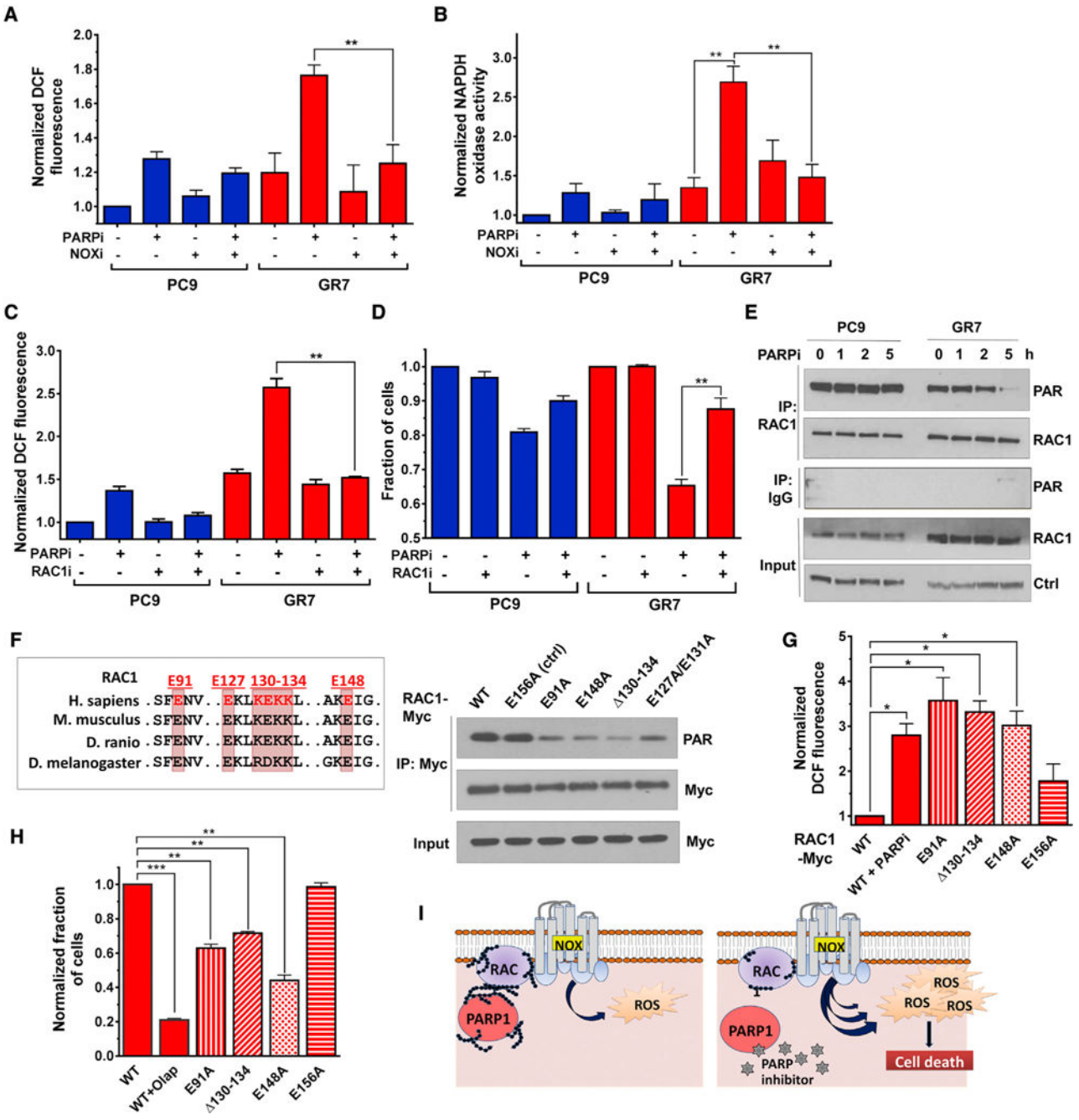

Figure 5. RAC1 Is PARylated by PARP-1 and Controls ROS Levels

(A) DCF fluorescence after 24-h treatment of TKI-S and TKI-R cells with olaparib or NOX inhibitor VAS-2870 (2 μM) as indicated, normalized to untreated TKI-S cells.

(B) NOX activity in TKI-S and TKI-R cells after drug treatments as indicated.

(C) Normalized DCF fluorescence in TKI-S and TKI-R cells following treatment with olaparib (5 μM) or RAC1 inhibitor NSC23766 (RACi) (25 μM).

(D) Fraction of cells after 5-day treatment of cells with drugs as indicated.

(E) Lysates from TKI-S and TKI-R cells treated with olaparib for 0 to 5 h were subjected to immunoprecipitation (IP) in which RAC1 immunoprecipitates were probed for PAR and for RAC1 itself.

(F) Left, sequence alignment of RAC1 protein from different species using clustalW. Conserved amino acids are indicated as well as mutated sequences for mutational analysis. Right, western blot showing expression and PARylation of myc-tagged RAC1 PARylation mutants in PC9 GR7 cells. WT, wild-type RAC1 sequence; E156A, glutamine mutant that does not affect parylation and serves as positive control (ctrl).

(G) DCF fluorescence of PC9 GR7 cells transfected with myc-tagged RAC1 constructs as shown, with or without olaparib (PARPi) treatment of cells expressing wild-type (WT) RAC1.

(H) Fraction of cells surviving after transfection of PC9 cells with the respective PARylation mutants compared to PARPi treatment.

(I) Model of PARP-1 as gatekeeper in EGFR mutant NSCLC cells treated with TKI where it restricts the production of cytotoxic ROS through PARylation of RAC1. Whether RAC1 is PARylated by a cytoplasmic PARP-1 fraction or in the nucleus remains to be determined.

Data points and error bars represent means with SE based on ≥3 biological repeats with ≥3 technical repeats.

*$p \leq 0.05$, **$p \leq 0.01$, ***$p \leq 0.001$.

See also Figures S8, S9, and S10.

KEY RESOURCES TABLE

REAGENT or RESOURCE	SOURCE	IDENTIFIER
Antibodies		
Anti-γ-H2AX (Ser139) (mouse monoclonal)	Millipore	Cat# 05-636; RRID:AB_310795
Anti-53BP1 (rabbit polyclonal)	Abcam	Cat# ab21083; RRID:AB_722496
Anti-PCNA (rabbit polyclonal)	Abcam	Cat# ab2426; RRID:AB_303062
Anti-PCNA (PC10) (mouse monoclonal)	Abcam	Cat# ab29; RRID:AB_303394
Anti-8-oxoguanine (mouse monoclonal)	Millipore	Cat# MAB3560; RRID:AB_94925
Anti-Rad51 (Ab-1) (rabbit polyclonal)	Millipore	Cat# PC130; RRID:AB_2238184
Anti-EGFR (1F4) (mouse monoclonal)	Cell Signaling	Cat# 2239S; RRID:AB_331373
Anti-PARP-1 (F-2) (mouse monoclonal)	Santa Cruz	Cat# sc-8007; RRID:AB_628105
Anti-XRCC1 (rabbit polyclonal)	Cell Signaling	Cat# 2735S; RRID:AB_2218471
Anti-PAR (monoclonal)	Trevigen	Cat# 4335-MC-100; RRID:AB_2572318
Anti-RAC1 (23A8)	Millipore	Cat# 05-389; RRID:AB_309712
HRP-conjugated rabbit anti-mouse	Santa Cruz	Cat# sc-358914; RRID:AB_10915700
HRP-conjugated goat anti-rabbit	Santa Cruz	Cat# sc-2030; RRID:AB_631747
Alexa Fluor 488 goat anti-mouse	Invitrogen	Cat# A11029; RRID:AB_138404
Alexa Fluor 555 goat anti-rabbit	Invitrogen	Cat# A21428; RRID:AB_141784
Mouse TrueBlot ULTRA: Anti-Mouse Ig HRP	Rockland antibodies and assays	Cat# 18-8817-30; RRID:AB_2610849
Anti-NRF2 (C-20) (rabbit polyclonal)	Santa Cruz	Cat# sc-722; RRID:AB_2108502
Biological Samples		
Tumor tissue explants from NSCLC patients	MGH	2012P002255
Chemicals, Peptides, and Recombinant Proteins		
Veliparib (ABT-888)	LC Laboratories	V-4703
Rucaparib	Selleckchem	S1098
Olaparib	LC Laboratories	AZ-2281
Niraparib	Selleckchem	MK-4827
Gefitinib	LC Laboratories	G-4408
Osimertinib	LC Laboratories	AZD9291
Diphenyleneiodonium	Sigma Aldrich	D2926
VAS-2870	Sigma Aldrich	SML0273
NSC 23766	Selleckchem	S8031
CellROX™ Green Reagent	Invitrogen	C10444
H2DCF-DA	Invitrogen	C6827
Critical Commercial Assays		
CometAssay® single cell gel electrophoresiskit	Trevigen	4250-050-K
OxyBlot Protein Oxidation Detection Kit	Millipore	S7150
Annexin V-Cy5 kit	BioVision	K103-100
X-tremeGENE siRNA Transfection Reagent	Roche	04476093001
QuickChange Mutagenesis Kit	Stratagene	200519
Experimental Models: Cell Lines		

REAGENT or RESOURCE	SOURCE	IDENTIFIER
MGH 119-1, 121-1, 134-1	Crystal et al., 2014	N/A
PC9, GR7	Sharma et al., 2010	N/A
PC9 B, C	Hata et al., 2016	N/A
HCC827, GR6	Engelman et al., 2007	N/A
HCC4006, GR6	Soucheray et al., 2015	N/A
H3255, GR	Engelman et al., 2006	N/A
Experimental Models: Organisms/Strains		
Female athymic nude (Nu/Nu) mice	Charles River	N/A
Oligonucleotides		
siRNA against PARP-1, validated	Santa Cruz	sc-29437
siRNA against XRCC1, validated	Ambion	121593
siRNA against RAC1, validated	Sigma Aldrich	EHU075591
Software and Algorithms		
TriTek CometScore	Tritek Corp	N/A
GraphPad Prism 6	GraphPad Software	N/A